nature materials

ARTICLES

https://doi.org/10.1038/s41563-021-00921-8

Highly stretchable multilayer electronic circuits using biphasic gallium-indium

Shanliangzi Liu[1,2], Dylan S. Shah[1] and Rebecca Kramer-Bottiglio[1]✉

Stretchable electronic circuits are critical for soft robots, wearable technologies and biomedical applications. Development of sophisticated stretchable circuits requires new materials with stable conductivity over large strains, and low-resistance interfaces between soft and conventional (rigid) electronic components. To address this need, we introduce biphasic Ga–In, a printable conductor with high conductivity (2.06×10^6 S m^{-1}), extreme stretchability (>1,000%), negligible resistance change when strained, cyclic stability (consistent performance over 1,500 cycles) and a reliable interface with rigid electronics. We employ a scalable transfer-printing process to create various stretchable circuit board assemblies that maintain their performance when stretched, including a multilayer light-emitting diode display, an amplifier circuit and a signal conditioning board for wearable sensing applications. The compatibility of biphasic Ga–In with scalable manufacturing methods, robust interfaces with off-the-shelf electronic components and electrical/mechanical cyclic stability enable direct conversion of established circuit board assemblies to soft and stretchable forms.

Soft and stretchable electronics are being integrated into next-generation electronic devices in a broad range of emerging fields, including soft robotics[1], wearable electronics[2], biomedical devices[3] and human–machine interfaces[4,5]. Encouraging progress has been made in developing novel materials and architectures for stretchable sensors[6], displays[7], heaters[8], energy storage devices[9] and integrated circuits (ICs)[10]. However, the field still lacks highly stretchable, multilayer electronic circuits with integrated computation, efficient data transmission and minimal electrical losses. Commercial electronics can provide a wide range of unobtrusive, inexpensive, high-performance ICs, ranging from microcontrollers to amplifiers, but creating stretchable circuits with these ICs requires a robust interface between each circuit element. In this work, we present stretchable versions of conventional printed circuit board (PCB) assemblies by employing a biphasic gallium-indium alloy (bGaIn) to create highly stretchable conductive traces and robust interfaces between soft and rigid electronic components.

Three main strategies are being actively researched to enable stretchable electronics: structure-based stretchable conductors, intrinsically stretchable conductors and conductive composites. Highly conductive, inextensible thin metal films can be geometrically patterned to gain out-of-plane deformability and linear stretchability[10–13]. Although they interface well with traditional electronic components, their stretchability and component areal density are often limited. Intrinsically stretchable conductors—such as room temperature liquid metals (eutectic gallium-indium, eGaIn[14]), ionic conductors[15] and conducting polymers[16,17]—do not require sophisticated patterning, but each suffers from several drawbacks, including leaking, dehydration, embrittlement and low conductivity. Conductive inclusion polymer composites are also stretchable without complex patterning, but usually suffer from low maximum strains and high resistance[18,19]. Further, there are relatively few reports on stretchable conductors that exhibit minimal resistance change during strain[20,21].

Much effort has been devoted to making reliable junctions between stretchable parts and commercially available, high-performance ICs. One popular approach, placing conventional electronic components onto strain-isolating (rigid) islands[10,22], reduces both the stretchability and durablilty of the resulting circuits. Another approach uses liquid metal droplets or solder paste to make temporary connections, but the stretchability of these solutions is usually limited to less than 100%, without consistent cyclic performance[23–27]. Taken together, a facile and scalable process to attain both strain-insensitive stretchable conductors and reliable conductor–component interfaces under large repetitive strain is still missing.

Here, we introduce biphasic Ga–In (bGaIn), a printable, solid–liquid biphasic material that maintains a near-constant resistance under extreme strains; maintains direct, consistent and stretchable electrical connections with conventional electronic components; and is mechanically stable when applied onto numerous soft materials. bGaIn is produced by thermally treating eGaIn nanoparticles to create a mixture of liquid and crystalline solids. It shows a high initial conductivity of 2.06×10^6 S m^{-1} and near-constant resistance at strains over 1,000%. We employ bGaIn as a stretchable interconnect to interface with commercial electronic components, including resistors, capacitors, light-emitting diodes (LEDs), operational amplifiers and microcontrollers, by simply pressing the electronics into the bGaIn trace. We demonstrate this facile and scalable approach with a highly stretchable amplifier circuit (Fig. 1a) and a 'YALE' LED array (Fig. 1b). Using bGaIn vertical interconnect accesses (VIAs) to connect traces on the top and bottom layers, we convert conventional multilayer PCB designs into stretchable circuit board assemblies (SCBAs) that maintain performance while experiencing large strains. We demonstrate the utility of these VIAs with a multilayer LED display (Fig. 1c) and a smart sensing garment (Fig. 1d,e). bGaIn is a simple, non-toxic, single-material solution for making stretchable conductors with robust interfaces to conventional electronic components, opening up opportunities to mass-manufacture stretchable circuits for a wide range of industrial applications, including soft displays and smart garments.

Material characteristics

eGaIn has emerged as a favourable material for stretchable electronics due to its high conductivity, intrinsic stretchability and printability[14].

[1]School of Engineering and Applied Science, Yale University, New Haven, CT, USA. [2]School of Mechanical Engineering, Purdue University, West Lafayette, IN, USA. ✉e-mail: rebecca.kramer@yale.edu

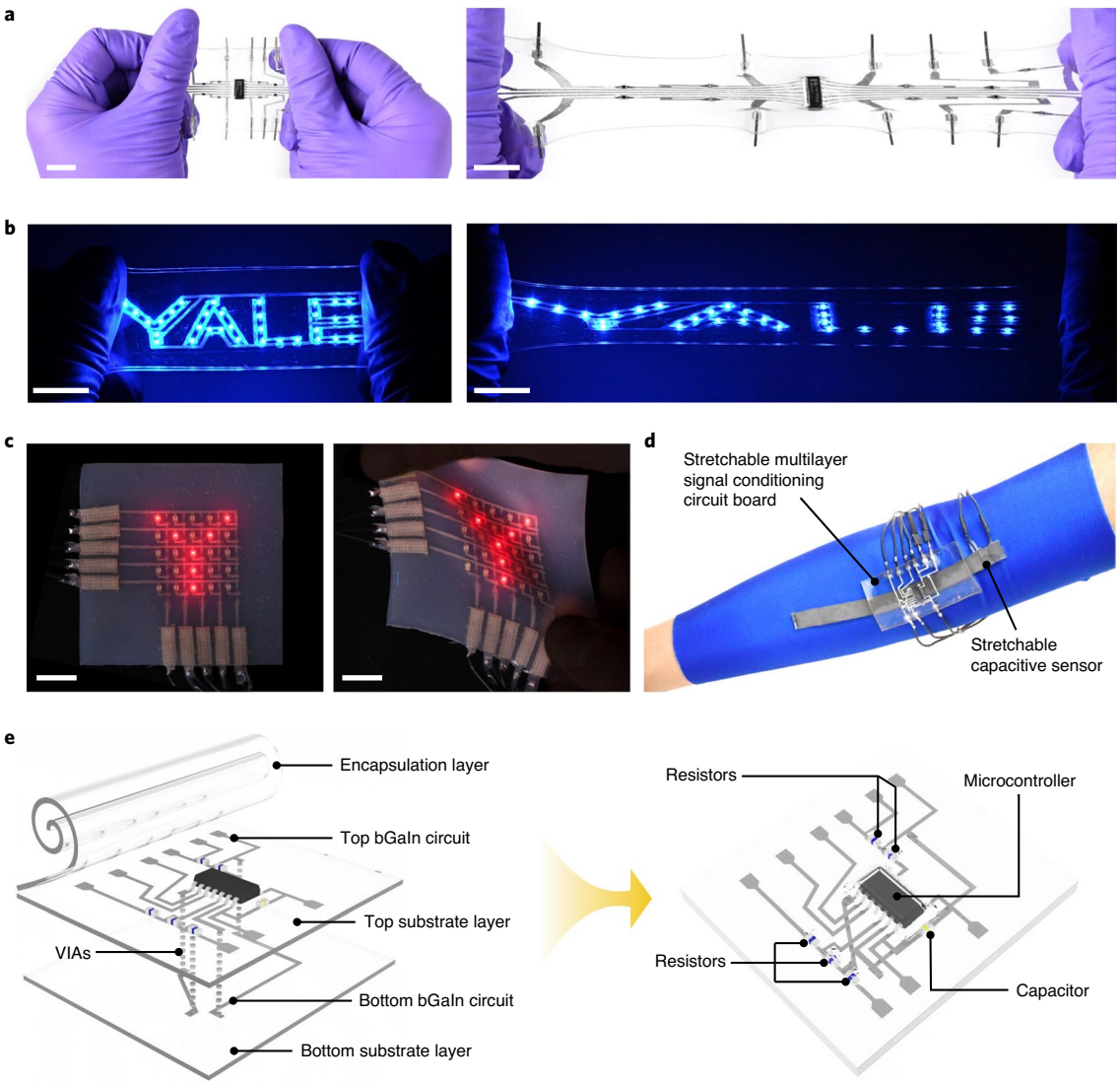

Fig. 1 | bGaIn for SCBAs. a, Amplifier circuit before and after stretching to 400% strain. **b**, 'Yale' LED array before and after stretching to 250% strain. **c**, Multilayer LED display before and after diagonal stretching. **d**, Multilayer signal conditioning circuit board integrated with a stretchable capacitive sensor attached to the surface of a user's shirt sleeve. **e**, Illustration of the circuit board in **d**. The encapsulation and substrate layers are 3M VHB tape. Scale bars, 1 cm (**a**–**c**).

When exposed to oxygen, eGaIn develops a near-instantaneous gallium oxide layer composed primarily of Ga_2O_3 (ref. [28]), which allows liquid metal to adhere to surfaces and adopt stable non-spherical shapes[29], but also imparts high surface tension (~624 mN m^{-1})[30], making the material challenging to process. To overcome the limitations posed by the large surface tension of liquid metal, we previously created liquid metal nanoparticle inks by sonicating bulk eGaIn in ethanol, and then printed those inks into thin films[31]. The electrically insulating oxide layer prevents spontaneous particle coalescence and makes the film non-conductive. To reactivate the liquid metal in micrometre-scale traces, we used a laser[31] to rupture the oxide skins of the nanoparticles and coalesce them into conductive paths. However, we discovered that, due to severe oxidation and phase segregation, high-temperature thermal sintering (another common sintering approach) often depletes the liquid cores of the nanoparticles, creating a pure solid film[32,33]. Fortunately, this technique paved the way for the creation of bGaIn via a general thermal treatment of the nanoparticles (Fig. 2a).

We made bGaIn by spray-printing a thick layer of eGaIn nanoparticles onto silicon (Fig. 2a,i), heating the deposited film in an enclosed furnace for 30 min at 900 °C (Supplementary Note 1) and then cooling the film in ambient conditions. This thermal sintering transforms the eGaIn nanoparticles into a thin solid film on top (~500 nm, invariant with respect to the original layer thickness) and a thick biphasic portion (~24 μm) with solid particles embedded in liquid eGaIn. During heating, the particles at the top surface transform into heterogeneously structured crystalline solids due to oxidation and phase segregation[33] (Fig. 2a(ii),b(i–iii) and Supplementary Fig. 1). The dense oxide layer largely prevents further oxygen penetration into the particles that lie deeper in the film, hence the consistent thickness. Meanwhile, the liquid particles underneath this solid layer experience large internal thermal stresses, owing to a larger thermal expansion of the liquid cores relative to the oxide shells[33], rupturing the oxide skins and coalescing the particles (Fig. 2a(iii),b(iv)). Once the bGaIn film was made, we transferred it to stretchable substrates (such as acrylic-based tape (VHB, 3M) or silicone elastomer (Dragon Skin, Smooth-On)) by pressing the silicon wafer onto the substrate. The solid film adheres to the substrate, and the biphasic portion remains on the surface (Fig. 2a(iv)). Although the bGaIn film initially con-

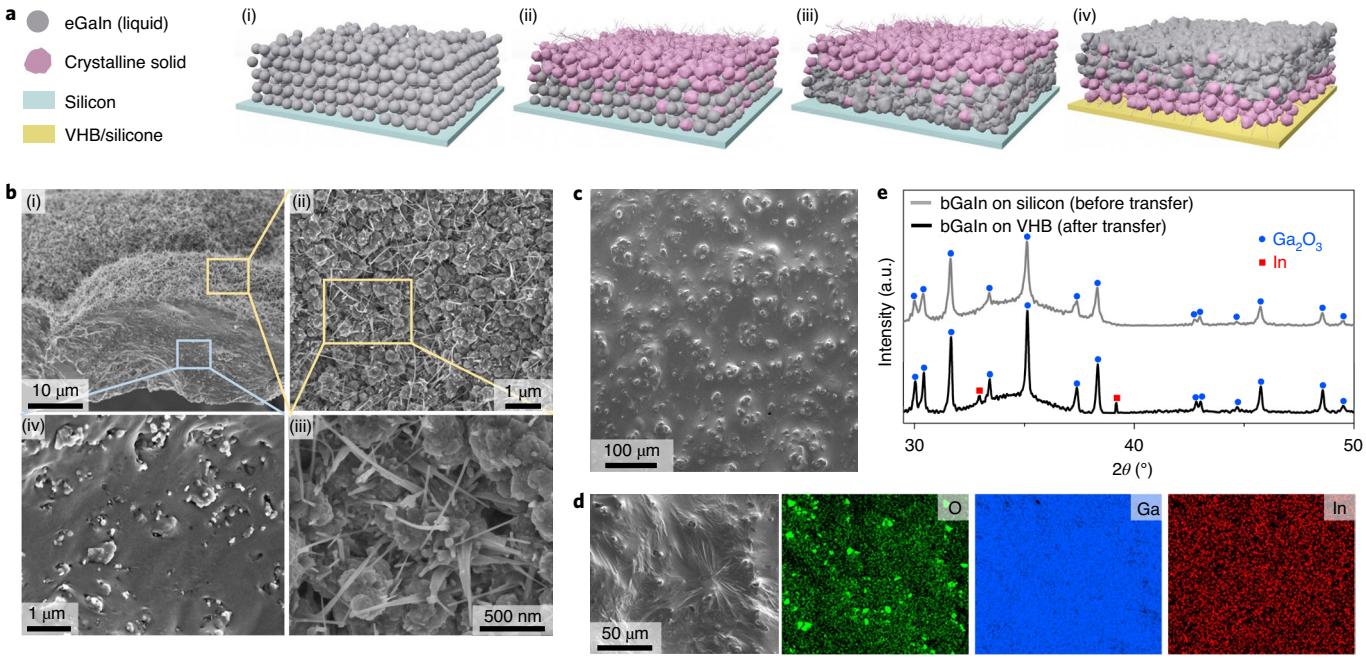

Fig. 2 | Material characteristics of bGaIn. a, Illustration of the process used to create and print bGaIn: eGaIn nanoparticles are spray printed onto a silicon wafer (i); during thermal sintering, particles at the top surface form heterogeneously structured crystalline solids (ii); below the solid film, a small number of particles are oxidized into solids (primarily Ga_2O_3), while the majority of the eGaIn particles coalesce into a conductive liquid (iii); the resulting bGaIn is transferred to a stretchable substrate (VHB/silicone; iv). **b**, Scanning electron microscopy images showing the cross-section of a bGaIn film, including the top solid film at various length scales (i–iii) and the biphasic portion (iv). **c**, Scanning electron microscopy image of the top surface of a bGaIn film after transferral to VHB tape. **d**, Energy dispersive spectroscopy mappings of the top surface of the bGaIn film after transfer, indicating higher oxygen concentrations in the areas with solid particles. **e**, X-ray diffraction patterns of the bGaIn film on a silicon wafer (before transferring to a soft substrate) and on VHB (after transfer).

tained some solids, this transfer process embeds additional solid particles into the biphasic portion (Fig. 2c and Supplementary Fig. 2). These solid particles exhibit higher oxygen concentrations than the liquid in the energy dispersive spectroscopy mappings (Fig. 2d and Supplementary Figs. 3–6), indicating a higher extent of oxidation. X-ray diffraction analysis shows that these solids are primarily monoclinic β-Ga_2O_3 crystals (Fig. 2e and Supplementary Note 2).

Electromechanical response

To establish a baseline of the electromechanical performance of bGaIn, we measured the relative resistance change (R/R_0) of bGaIn traces undergoing uniaxial tensile strain on multiple stretchable substrates. The traces had exceptionally stable electrical performance, experiencing negligible resistance change at both 100% strain on silicone elastomer (polydimethylsiloxane (PDMS); $R/R_0 \approx 1.06$; Fig. 3a) and 500% strain on VHB ($R/R_0 \approx 1.81$; Fig. 3b). These values are notably smaller than the theoretical prediction for a classical incompressible, constant-conductivity bulk liquid metal conductor using Pouillet's law, which exhibits large increases in resistance even at moderate strains ($R/R_0 = (1+\epsilon)^2$, where ϵ is the applied strain; Fig. 3a,b, black; $R/R_0 = 4$ at 100% strain on PDMS, 36 at 500% strain on VHB; experimental validation in Supplementary Fig. 7). At strains over 1,000%, the resistance increased less than five times (Supplementary Fig. 8), but strains of ~1,200% typically resulted in mechanical failure of the VHB substrate. Furthermore, we subjected bGaIn traces to cyclic strains of 100% (Fig. 3c) on PDMS and 500% on VHB (Fig. 3d). After moderate settling during the initial cycles, the bGaIn attained stable electromechanical behaviour over 1,500 loading cycles. We hypothesize this is due to rearrangement of the solid particles, from a random or non-uniform distribution caused by the transfer process, into a more uniform distribution induced by stretching. Compared to state-of-the-art stretchable conductors, bGaIn has outstanding performance in its high initial conductivity (2.06×10^6 S m^{-1}), extreme stretchability (>1,000%) and negligible resistance change over strains (Fig. 3e,f).

Due to the scattered solid oxide particles being primarily semiconductive Ga_2O_3, the initial conductivity of bGaIn (2.06×10^6 S m^{-1}) is lower than that of bulk eGaIn (3.40×10^6 S m^{-1}). As a bGaIn trace is stretched on a substrate, the liquid portion of it decreases in thickness to compensate for the increase in trace length. We hypothesize that the thickness of the embedded solid particles quickly exceeds the thickness of the liquid during strain, and therefore the solid particles begin to emerge from the liquid. Thus, the volume of the solid particles completely immersed in the liquid decreases with increasing strain. When the system is relaxed, the solid particles are resubmerged in the liquid. This mechanism results in increasing conductivity of the bGaIn trace with increasing strain, which is offset by the decreasing cross-sectional area of the trace and results in stable trace conductance during strain (Supplementary Note 3).

The unique electromechanical behaviour of bGaIn also relies upon the wettability of the liquid metal to the solid oxide particles. A previous approach to fabricating similar biphasic alloys involves mixing solid particles with liquid eGaIn, which typically results in poor adhesion between the liquid and solid components and consequently large resistance increases under strain[34–36]. Here, the thermal sintering process generates solid particles from within the liquid metal, allowing the liquid to wet the solid particles and encouraging it to percolate through their interstices (Supplementary Fig. 9). This superior wettability reduces separation between solid and liquid in the biphasic material, and therefore promotes continuous, high conductivity. The solid particles

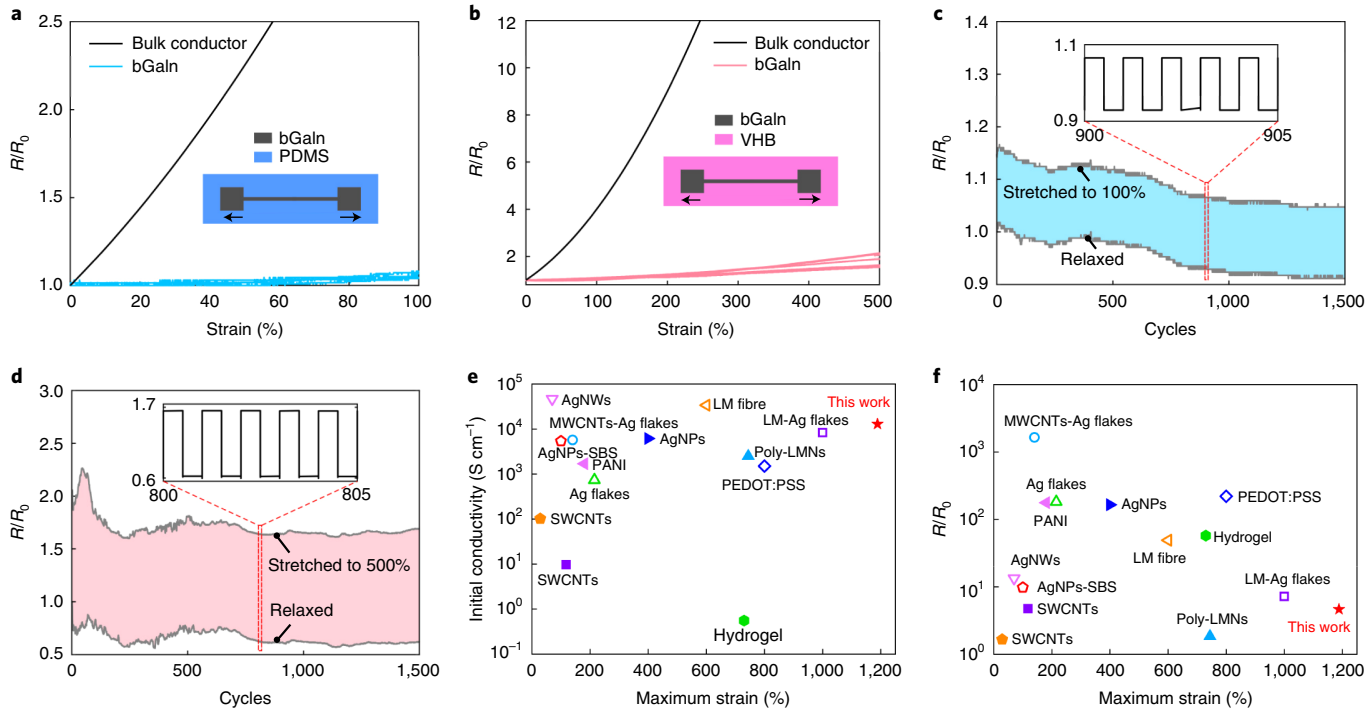

Fig. 3 | Electromechanical characteristics of bGaIn. a,**b**, Relative change in resistance as a function of uniaxial tensile strain of the bGaIn traces on PDMS (blue, **a**, $R/R_0 \approx 1.06 \pm 0.016$, four samples) and VHB (pink, **b**, $R/R_0 \approx 1.81 \pm 0.26$, six samples), and theoretical prediction based on bulk conductor assumptions (black). The insets illustrate top views of the samples. **c**,**d**, Relative resistance change of the bGaIn traces subjected to uniaxial tensile cyclic loading to 100% on PDMS (blue, **c**) and 500% on VHB (pink, **d**) up to 1,500 cycles. The insets show detailed electrical resistances as a response to uniaxial strains. **e**,**f**, Comparison of initial conductivity (0% strain) and stretchability (**e**), as well as relative resistance change at maximum strain (**f**) with other stretchable conductors: Ag flakes in fluorine rubber (Ag flakes)[18], Ag nanoparticles in fluorine rubber (AgNPs)[44], Ag nanoparticles in poly(styrene-block-butadieneblock-styrene) rubber fibres (AgNPs-SBS)[45], Ag nanowires (AgNWs)[46], poly(3,4-ethylenedioxythiophene):poly(styrenesulfonate) (PEDOT:PSS)[16], liquid metal fibre (LM fibre)[47], liquid metal Ag flakes in ethylene-vinyl acetate (EVA) (LM-Ag flakes)[20], single-walled carbon nanotubes (SWCNTs)[48], polyaniline (PANI)[17], polymerized liquid metal networks (Poly-LMNs)[21], multi-walled carbon nanotubes and Ag flakes in polyvinylidenefluoride copolymer (MWCNTs-Ag flakes)[49] and polyacrylamide hydrogel (Hydrogel)[15].

adhere to the substrate throughout stretching, while maintaining adhesion to the liquid metal and preventing the formation of electrically isolated liquid droplets (Supplementary Fig. 10). Supplementary Video 1 shows the solid side of the bGaIn film breaking into flakes when stretched, while the biphasic portion fills in the cracks, maintaining connection between the solid particles, which allows the bGaIn film to remain thin and continuous on the substrate during stretching.

Integration with rigid electronic components

With the baseline behaviour of bGaIn characterized, we now show that it creates robust electrical connections with rigid electronics. Reliably interfacing liquid metal with rigid electronics is challenging, and the few existing examples of liquid metal based SCBAs require cumbersome fabrication processes that are not compatible with current scalable manufacturing methods[23,24,26]. Further, state-of-the-art stretchable conductors have not been shown to directly interface with rigid electronics[21,37]. Here, we employ bGaIn as a stretchable interconnect to achieve reliable interfaces with rigid electronic components.

First, we used the transmission line method[38] to measure the contact resistance between bGaIn and (equivalently) zero-ohm-resistance, tinned copper contacts. By varying the length of the bGaIn traces (the space between adjacent tinned copper contacts), measuring the total resistance between bars and fitting a line to the data (Fig. 4a; coefficient of determination, $R^2 = 0.9986$), we calculated the contact resistance (half of the y intercept) to be 0.06 Ω, an order of magnitude lower than other liquid metal based contacts previously reported[39] (Supplementary Note 4).

After measuring the contact resistance, we interfaced a zero-ohm surface mount resistor with a bGaIn trace on various stretchable substrates, and measured the resistance change during strain. At 100% strain on PDMS (Fig. 4b), the R/R_0 value was approximately 1.40, and at 500% strain on VHB (Fig. 4c) the relative resistance was approximately 4.47. When pressing an electrical component onto patterned bGaIn traces, the oxide layers of the liquid metal break, and the bGaIn flows and encompasses the rigid pins, increasing contact area and reducing the contact resistance. The solid particles aid in securing the liquid to the rigid pin due to their natural inextensibility, their propensity to adhere to solid surfaces and the strong wettability to them by the liquid (Fig. 4d, Supplementary Fig. 11 and Supplementary Video 1), resulting in stable electrical connections during and after stretching. This electromechanical sensitivity to strain is low compared to the prediction based on bulk conductor assumptions (Fig. 4e black) and other liquid metal based interfacing approaches (Fig. 4e). Furthermore, the bGaIn traces with an embedded zero-ohm resistor subjected to a repetitive strain of 100% (Fig. 4f) on PDMS and 500% on VHB (Fig. 4g) remained functional over 1,500 loading cycles. Additional strain tests on bGaIn traces with and without embedded zero-ohm resistors on both PDMS and VHB substrates verified their stable performance at various strain rates (150 mm min^{-1}, 225 mm min^{-1} and 300 mm min^{-1}) for 1,000 loading cycles (Supplementary Fig. 12). Further, traces aged for over six months in standard laboratory conditions (23 °C and 50%

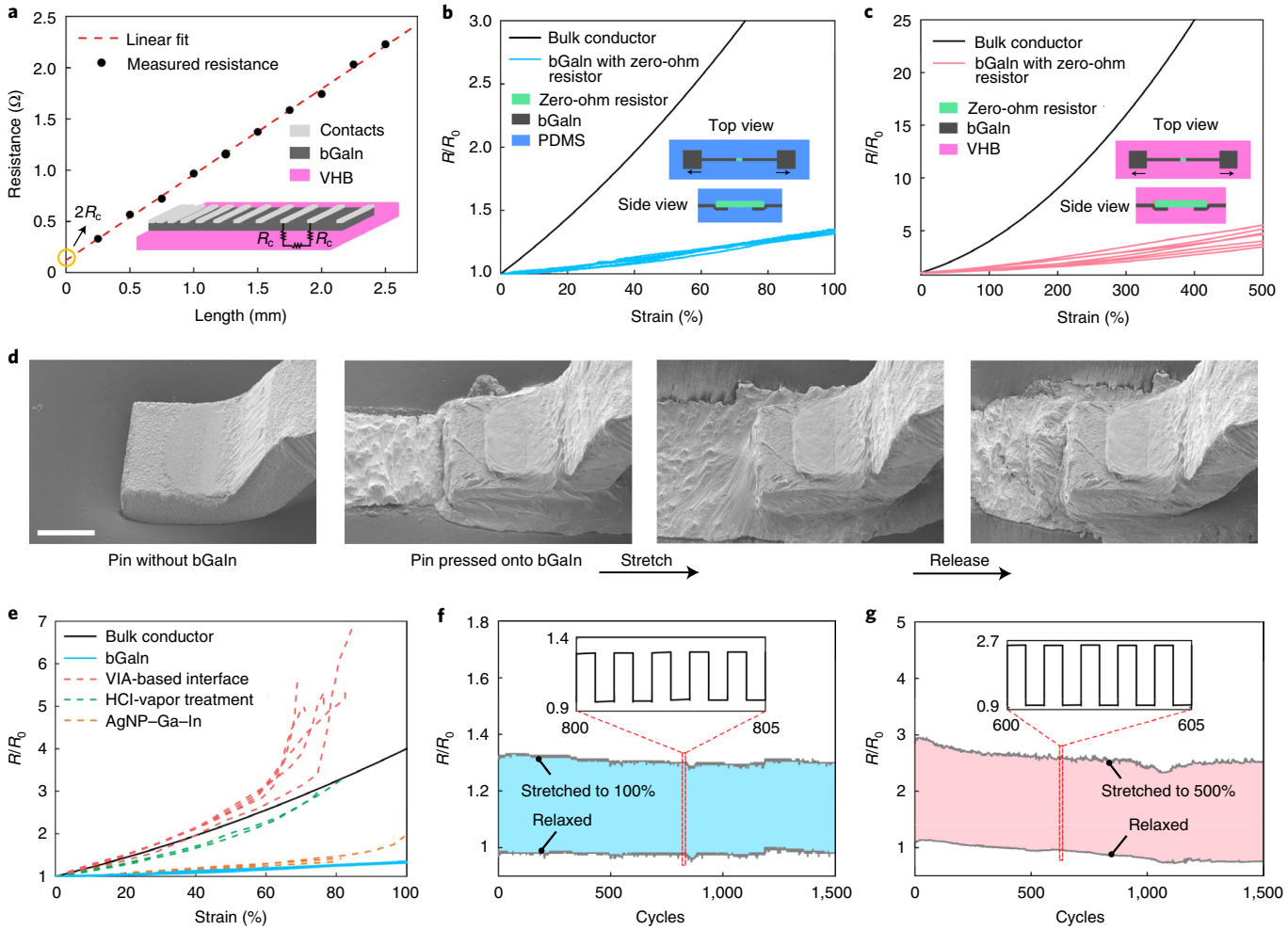

Fig. 4 | Integration with rigid electronic components. a, Contact resistance measurement for a bGaIn–component interface using the transmission line method ($R_c = 0.06\,\Omega$, $R^2 = 0.9986$). The inset shows the schematic of the samples for the contact resistance measurement. **b**,**c**, Relative change in resistance as a function of uniaxial tensile strain of the bGaIn traces with embedded zero-ohm resistor on PDMS (blue, **b**, $R/R_0 \approx 1.40 \pm 0.1$, five samples) and VHB (pink, **c**, $R/R_0 \approx 4.47 \pm 0.77$, seven samples), and theoretical prediction based on bulk conductor assumptions (black). The insets illustrate top and side views of the samples. **d**, Scanning electron microscopy images showing microstructure of a bGaIn–component interface at different stretching states (unstretched, stretched to 30% and released). The leftmost image of the electronic pin is included as a comparison. Scale bar, 200 μm. **e**, Comparison of relative resistance change over strains with other liquid metal based interfacing approaches: AgNP-Ga-In (ref. [50]), HCl-vapour treatment[24] and VIA-based interface[26]. **f**,**g**, Relative resistance change of the bGaIn traces with embedded zero-ohm resistor subjected to uniaxial tensile cyclic loading to 100% on PDMS (blue, **f**) and 500% on VHB (pink, **g**), up to 1,500 cycles. The insets show detailed electrical resistances as a response to uniaxial strains.

humidity) exhibited no evidence of long-term electromechanical degradation (Supplementary Fig. 13).

Printable patterns and stretchable VIAs

Patterning thin films of bulk eGaIn is challenging since its high surface tension causes the liquid metal to bead up and deviate from the desired deposition pattern[40]. By contrast, the solid particles in bGaIn spread evenly over the printed area, and then strong wetting between the liquid metal and the crystalline particles stabilizes the liquid, preventing unwanted beading. This mechanical stability helps bGaIn to work well with a variety of trace manufacturing processes. The main fabrication process that we use is transfer-printing by simply pressing a silicon wafer, on which bGaIn was made, onto a masked, stretchable substrate. Alternatively, we turned bGaIn into a conductive, printable paste by scraping bGaIn off the silicon wafer and mechanically mixing the top oxide into the biphasic portion. We used the paste to stencil-print and hand-write stretchable patterns on a variety of substrates, including VHB tape (Fig. 5a), paper (Fig. 5b), high-porosity foam (Fig. 5c) and latex balloon (Fig. 5d). Through these two techniques, we show facile printing of thin (<20 μm) bGaIn films.

The bGaIn paste can be filled into laser-cut cavities to easily create stretchable VIAs. The bGaIn strongly wets and adheres to the cavity, bridging the top and bottom traces (Supplementary Fig. 14), even when stretched (Supplementary Fig. 15). We measured the electrical resistance of circuits with a single VIA connecting two bGaIn traces at high strains (Fig. 5e). The relative resistance at 500% strain on VHB was 2.03, which remains notably lower than the theoretical prediction based on bulk conductor assumptions (Fig. 3a black; $R/R_0 = 36$ at 500%). The electromechanical response of a VIA strained cyclically to 500% on VHB also remained consistent over 1,500 loading cycles (Fig. 5f).

SCBAs

We made various SCBAs that demonstrate the near-universal utility of bGaIn to create stretchable soft robotic and wearable electronics.

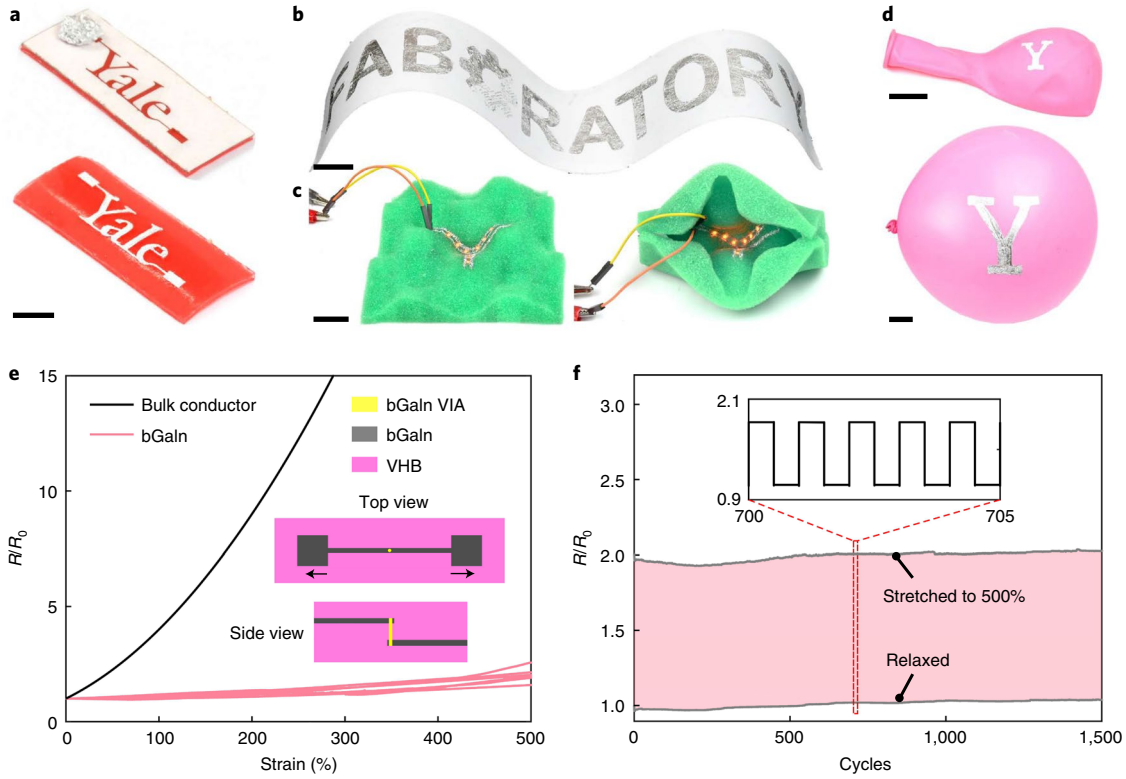

Fig. 5 | Printable patterns and stretchable VIAs. a,**b**, Stencil-printed bGaIn circuits on VHB tape (**a**; scale bar, 5 mm) and paper (**b**; scale bar, 2 cm). **c**,**d**, Hand-written bGaIn circuits on high-porosity foam (**c**) and a latex balloon (**d**); scale bar, 2 cm. **e**, Relative change in resistance as a function of uniaxial tensile strain of two bGaIn traces connected by a single VIA on VHB (pink, $R/R_0 \approx 2.03 \pm 0.32$, six samples) and theoretical prediction based on bulk conductor assumptions (black). The inset illustrates top and side views of the samples. **f**, Relative resistance change of two bGaIn traces connected by a single VIA subjected to uniaxial tensile cyclic loading to 500% on VHB up to 1,500 cycles. The inset shows detailed electrical resistances as a response to uniaxial strains.

We first stretched a 'YALE' LED array (bGaIn electrical interconnects, 33 LEDs pick-and-place assembled) on VHB tape to 250% strain (Fig. 1b and Supplementary Video 2), with no perceptible diminishing of the LED brightness. We then made an SCBA with a non-inverting summing amplifier circuit (Figs. 1a and 6a, and Supplementary Fig. 16). The output voltage (V_{out}) of the representative summing circuit is proportional to the sum of the input voltages (V_{in1} and V_{in2}), as $V_{out} = \frac{(R_3 + R_4)}{2 \times R_3} \times (V_{in1} + V_{in2})$, and is therefore highly sensitive to large resistance changes in the circuit. Initially, when supplied with a 100 mV peak-to-peak voltage (100 mV_{pp}) sinusoidal signal with a 100 mV offset on both V_{in1} and V_{in2}, the circuit produced the expected output voltage (1.1 V_{pp}; Fig. 6b), closely matching the results obtained with the same circuit built on a rigid PCB. Furthermore, stretching the circuit to different strains had a negligible impact on the output signal (Fig. 6b and Supplementary Video 3). Finally, the measured amplitude and phase shift at different strains were approximately the same as the theoretical values (0.55 V; 0 rad).

To further clarify the utility of bGaIn in resistance-sensitive circuits, we also demonstrated a first-order resistor–capacitor low-pass filter circuit using bGaIn as electrical interconnects and compared it to an identical circuit manufactured using bulk eGaIn (Supplementary Fig. 17). The bGaIn circuit exhibited similar outputs and cut-off frequencies (~936 Hz) at various strain levels up to 400% strain, while the eGaIn circuit failed at less than 100% strain. The stable performance during these collective experiments proves the capability of bGaIn to enable SCBAs that retain their electrical performance over large strains.

After demonstrating single-layer bGaIn circuits, we used bGaIn VIAs to create multilayer, high-performance stretchable circuits. First, we made a stretchable LED display with 25 LEDs and 25 corresponding bGaIn VIAs arranged in a 5×5 grid (Fig. 1c). We built this circuit in silicone elastomer to demonstrate the transferrability of our manufacturing methods to non-adhesive substrates. The LEDs in the display could be controlled individually by an external microcontroller (Arduino Uno) to create a scrolling message, while being stretched along all in-plane strain directions (Supplementary Video 4).

Lastly, we made a multilayer signal conditioning circuit, with integrated sensing and computation, for wearable sensing applications. Typical wearable capacitive stretch sensors require a colocated, rigid signal conditioning circuit board for capacitance measurement[41], moderately constraining the movement of the body. We rebuilt this board as an SCBA on VHB tape, integrating a microcontroller, a capacitor and five resistors with transfer-printed bGaIn interconnects and bGaIn-filled VIAs (Fig. 1d,e, Fig. 6d,e and Supplementary Fig. 18).

We held the signal conditioning circuit board at a series of strains (0%, 50%, 100%, 150%, 200%), while subjecting the capacitive sensor to ten cycles of 50% strain (Fig. 6f). As expected, the signal conditioning board maintained a linear response when stretched up to 200%, with any deviations simply the result of sensor noise. We then directly integrated the stretchable capacitive sensor with the signal conditioning board and attached the sensor–circuit assembly to the surface of a shirt sleeve (Fig. 1d and Fig. 6g). The sensor and the circuit deformed simultaneously during elbow flexion, and the signal conditioning circuit measured the motion of the user's arm (Fig. 6g and Supplementary Video 5). In contrast to previous works where the sensing circuit was often placed outside the active region[42,43], here we were able to colocate the circuit and sensor directly over

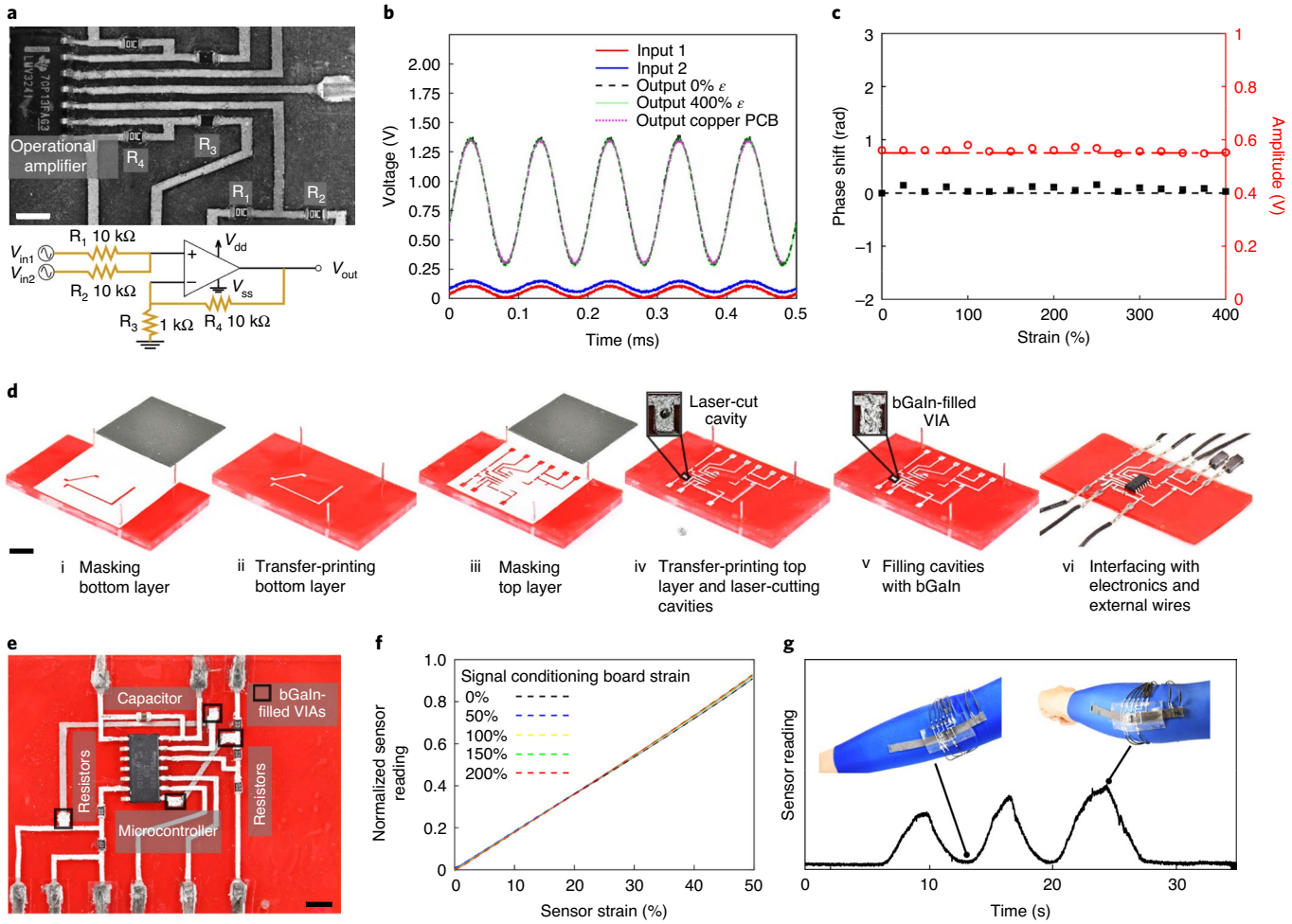

Fig. 6 | Applications of SCBAs. a, Top view and circuit diagram of the summing amplifier circuit. V_{dd} and V_{ss} are the drain and sink power voltage, respectively. R_1 and R_2 are the input resistors, R_3 is the grounded input resistor and R_4 is the feedback resistor. Scale bar, 1 mm. **b**, Input sinusoidal voltage signals (100 mV_{pp}, 100 mV_{pp} offset), along with output signals after amplification when the amplifier circuit is at 0% and 400% strain, as well as the same circuit built with copper traces as a control group. **c**, Phase shift and amplitude of the amplifier circuit output signals as a function of applied strain. The dash–dot line (red) and dashed line (black) represent the theoretical amplitude value (0.55 V) and phase shift (0 rad), respectively. **d**, Fabrication process of the multilayer signal conditioning circuit board. Scale bar, 1 cm. **e**, Top view of the signal conditioning circuit board. Scale bar, 5 mm. **f**, Normalized sensor reading as a function of the capacitive sensor strain up 50% for ten cycles at different strains of the signal conditioning circuit board (0%, 50%, 100%, 150%, 200%). Each shaded region represents ±1 s.d. about the mean (solid line). **g**, A stretch sensor and signal conditioning circuit board were attached to a spandex sleeve and stretched together during normal bending motions of a user's arm. The insets show this sensory sleeve while the user's arm is straight (left inset) and bent (right inset).

the user's elbow. This presents a key advance towards unobtrusive wearable electronics.

Outlook

In this work, we have introduced a material and fabrication method to rapidly produce SCBAs with excellent electrical performance and reliability. The bGaIn developed herein incorporates high initial conductivity (2.06×10^6 S m^{-1}), extreme stretchability past 1,000%, cyclic stability up to at least 1,500 cycles and negligible resistance change over strains. This material can directly interface with conventional electronic components to attain robust and stretchable electrical connections. The combination of these unique traits enables facile and direct conversion of sophisticated PCB assemblies into their corresponding SCBAs.

Resolution of the SCBAs fabricated using this approach is currently limited by the laser-cut masks (~25 µm). Appropriately tailoring the solid-to-liquid ratio of bGaIn could potentially create inks with improved physical properties for higher resolution, extrusion-based printing. Further research in optimizing bGaIn ink properties would enable scalable manufacturing of stretchable circuits with high integration densities. The potential applications and impact of this material are wide, including wearable health-monitoring devices for next-generation healthcare; intuitive, soft human–machine interfaces; and circuits with integrated sensing, actuation and distributed computation, for soft robotics.

Online content

Any methods, additional references, Nature Research reporting summaries, source data, extended data, supplementary information, acknowledgements, peer review information; details of author contributions and competing interests; and statements of data and code availability are available at https://doi.org/10.1038/s41563-021-00921-8.

Received: 28 May 2020; Accepted: 6 January 2021;
Published online: 18 February 2021

References

1. Rich, S. I., Wood, R. J. & Majidi, C. Untethered soft robotics. *Nat. Electron.* **1**, 102–112 (2018).
2. Liu, Y., Pharr, M. & Salvatore, G. A. Lab-on-skin: a review of flexible and stretchable electronics for wearable health monitoring. *ACS Nano* **11**, 9614–9635 (2017).
3. Rogers, J. A., Ghaffari, R. and Kim, D.-H. *Stretchable Bioelectronics for Medical Devices and Systems* (Springer, 2016).
4. Lim, S. et al. Transparent and stretchable interactive human machine interface based on patterned graphene heterostructures. *Adv. Funct. Mater.* **25**, 375–383 (2015).
5. Jeong, J.-W. et al. Materials and optimized designs for human-machine interfaces via epidermal electronics. *Adv. Mater.* **25**, 6839–6846 (2013).
6. Chen, D. & Pei, Q. Electronic muscles and skins: a review of soft sensors and actuators. *Chem. Rev.* **117**, 11239–11268 (2017).
7. Wang, J. & Lee, P. S. Progress and prospects in stretchable electroluminescent devices. *Nanophotonics* **6**, 435–451 (2016).
8. Bilodeau, R. A., Nasab, A. M., Shah, D. S. and Kramer-Bottiglio, R. Uniform conductivity in stretchable silicones *via* multiphase inclusions. *Soft Matter* https://doi.org/10.1039/D0SM00383B (2020).
9. Yan, C. & Lee, P. S. Stretchable energy storage and conversion devices. *Small* **10**, 3443–3460 (2014).
10. Huang, Z. et al. Three-dimensional integrated stretchable electronics. *Nat. Electron.* **1**, 473–480 (2018).
11. Gray, D. S., Tien, J. and Chen, C. S. High-conductivity elastomeric electronics. *Adv. Mater.* **16**, 393–397 (2004).
12. Rogers, J. A., Someya, T. & Huang, Y. Materials and mechanics for stretchable electronics. *Science* **327**, 1603–1607 (2010).
13. Miyamoto, A. et al. Inflammation-free, gas-permeable, lightweight, stretchable on-skin electronics with nanomeshes. *Nat. Nanotechnol.* **12**, 907–913 (2017).
14. Dickey, M. D. Stretchable and soft electronics using liquid metals. *Adv. Mater.* **29**, 1606425 (2017).
15. Keplinger, C. et al. Stretchable, transparent, ionic conductors. *Science* **341**, 984–987 (2013).
16. Wang, Y. et al. A highly stretchable, transparent, and conductive polymer. *Sci. Adv.* **3**, e1602076 (2017).
17. Stoyanov, H., Kollosche, M., Risse, S., Waché, R. & Kofod, G. Soft conductive elastomer materials for stretchable electronics and voltage controlled artificial muscles. *Adv. Mater.* **25**, 578–583 (2013).
18. Matsuhisa, N. et al. Printable elastic conductors with a high conductivity for electronic textile applications. *Nat. Commun.* **6**, 7461 (2015).
19. Tee, B. C. K. & Ouyang, J. Soft electronically functional polymeric composite materials for a flexible and stretchable digital future. *Adv. Mater.* **30**, 1802560 (2018).
20. Jiangxin, W. et al. Printable superelastic conductors with extreme stretchability and robust cycling endurance enabled by liquid-metal particles. *Adv. Mater.* **30**, 1706157 (2018).
21. Thrasher, C., Farrell, Z., Morris, N., Willey, C. & Tabor, C. Mechanoresponsive polymerized liquid metal networks. *Adv. Mater.* **31**, 1903864 (2019).
22. Kim, D.-H. et al. Epidermal electronics. *Science* **333**, 838–843 (2011).
23. Lu, T., Markvicka, E. J., Jin, Y. & Majidi, C. Soft-matter printed circuit board with UV laser micropatterning. *ACS Appl. Mater. Interfaces* **9**, 22055–22062 (2017).
24. Bugra, O. K., James, W., Burak, O. O. & Carmel, M. EGaIn–metal interfacing for liquid metal circuitry and microelectronics integration. *Adv. Mater. Interfaces* **5**, 1701596 (2018).
25. Matsuhisa, N., Chen, X., Bao, Z. & Someya, T. Materials and structural designs of stretchable conductors. *Chem. Soc. Rev.* **48**, 2946–2966 (2019).
26. Marques, D. G., Lopes, P. A., de Almeida, A. T., Majidi, C. & Tavakoli, M. Reliable interfaces for EGaIn multi-layer stretchable circuits and microelectronics. *Lab Chip* **19**, 897–906 (2019).
27. Biswas, S. et al. Integrated multilayer stretchable printed circuit boards paving the way for deformable active matrix. *Nat. Commun.* **10**, 4909 (2019).
28. Scharmann, F. et al. Viscosity effect on GaInSn studied by XPS. *Surf. Interface Anal.* **36**, 981–985 (2004).
29. Ladd, C., So, J.-H., Muth, J. & Dickey, M. D. 3D printing of free standing liquid metal microstructures. *Adv. Mater.* **25**, 5081–5085 (2013).
30. Zrnic, D. & Swatik, D. S. On the resistivity and surface tension of the eutectic alloy of gallium and indium. *J. Less Common Met.* **18**, 67–68 (1969).
31. Liu, S. et al. Laser sintering of liquid metal nanoparticles for scalable manufacturing of soft and flexible electronics. *ACS Appl. Mater. Interfaces* **10**, 28232–28241 (2018).
32. Cutinho, J. et al. Autonomous thermal-oxidative composition inversion and texture tuning of liquid metal surfaces. *ACS Nano* **12**, 4744–4753 (2018).
33. Liu, S., Reed, S. N., Higgins, M. J., Titus, M. S. & Kramer-Bottiglio, R. Oxide rupture-induced conductivity in liquid metal nanoparticles by laser and thermal sintering. *Nanoscale* **11**, 17615–17629 (2019).
34. Wu, Y.-h et al. A novel strategy for preparing stretchable and reliable biphasic liquid metal. *Adv. Funct. Mater.* **29**, 1903840 (2019).
35. Daalkhaijav, U., Yirmibesoglu, O. D., Walker, S. & Mengüç, Y. Rheological modification of liquid metal for additive manufacturing of stretchable electronics. *Adv. Mater. Technol.* **3**, 1700351 (2018).
36. Chang, H. et al. Recoverable liquid metal paste with reversible rheological characteristic for electronics printing. *ACS Appl. Mater. Interfaces* **12**, 14125–14135 (2020).
37. Markvicka, E. J., Bartlett, M. D., Huang, X. & Majidi, C. An autonomously electrically self-healing liquid metal–elastomer composite for robust soft-matter robotics and electronics. *Nat. Mater.* **17**, 618–624 (2018).
38. Reeves, G. K. & Harrison, H. B. Obtaining the specific contact resistance from transmission line model measurements. *IEEE Electron Device Lett.* **3**, 111–113 (1982).
39. Kim, S., Oh, J., Jeong, D. & Bae, J. Direct wiring of eutectic gallium–indium to a metal electrode for soft sensor systems. *ACS Appl. Mater. Interfaces* **11**, 20557–20565 (2019).
40. Joshipura, I. D., Ayers, H. R., Majidi, C. & Dickey, M. D. Methods to pattern liquid metals. *J. Mater. Chem. C* **3**, 3834–3841 (2015).
41. White, E. L., Yuen, M. C., Case, J. C. & Kramer, R. K. Low-cost, facile, and scalable manufacturing of capacitive sensors for soft systems. *Adv. Mater. Technol.* **2**, 1700072 (2017).
42. Bartlett, M. D., Markvicka, E. J. & Majidi, C. Rapid fabrication of soft, multilayered electronics for wearable biomonitoring. *Adv. Funct. Mater.* **26**, 8496–8504 (2016).
43. O'Brien, B., Gisby, T. and Anderson, I. A. Stretch sensors for human body motion. In *SPIE Proceedings Vol. 9056: Electroactive Polymer Actuators and Devices (EAPAD) 2014* (ed. Bar-Cohen, Y.) 905618 (International Society for Optics and Photonics, 2014).
44. Matsuhisa, N. et al. Printable elastic conductors by in situ formation of silver nanoparticles from silver flakes. *Nat. Mater.* **16**, 834–840 (2017).
45. Park, M. et al. Highly stretchable electric circuits from a composite material of silver nanoparticles and elastomeric fibres. *Nat. Nanotechnol.* **7**, 803–809 (2012).
46. Liang, J., Tong, K. & Pei, Q. A water-based silver-nanowire screen-print ink for the fabrication of stretchable conductors and wearable thin-film transistors. *Adv. Mater.* **28**, 5986–5996 (2016).
47. Zhu, S. et al. Ultrastretchable fibers with metallic conductivity using a liquid metal alloy core. *Adv. Funct. Mater.* **23**, 2308–2314 (2013).
48. Sekitani, T. et al. Stretchable active-matrix organic light-emitting diode display using printable elastic conductors. *Nat. Mater.* **8**, 494–499 (2009).
49. Chun, K.-Y. et al. Highly conductive, printable and stretchable composite films of carbon nanotubes and silver. *Nat. Nanotechnol.* **5**, 853–857 (2010).
50. Tavakoli, M. et al. EGaIn-assisted room-temperature sintering of silver nanoparticles for stretchable, inkjet-printed, thin-film electronics. *Adv. Mater.* **30**, 1801852 (2018).

Methods

Material fabrication. The liquid metal nanoparticle ink was made by adding 362 ± 5 mg of eGaIn alloy (75.5% Ga, 24.5% In; 495425, Sigma Aldrich) into 4 ml of ethanol (V1001, Koptec) and then sonicating at an amplitude of 36 µm (30% setting) for 120 min using a tip sonicator (1/16 inch microtip probe, QSonica Q700). Prior to spray-printing, the ink was mixed vigorously using a vortex mixer (VortexGenie) for 3 min to ensure uniform dispersion. The nanoparticle ink was then sprayed onto a silicon wafer substrate using a customized spray printer. Compressed air (20 psi) was blown over a syringe needle while ink was dispensed at a fixed rate (0.3 ml min^{-1}), with the printer stage translating underneath at 5 mm s^{-1}. A 3 ml syringe of ink made a single layer of film, with the process being repeated ten times to create films thick enough for bGaIn to form. After spray deposition, the printed liquid metal nanoparticle film was heated in a furnace (Lindberg/Blue M BF51766A-1, Thermo Fisher Scientific) at 900 °C for 30 min and then cooled in ambient conditions.

After the thermal sintering, stretchable substrates such as VHB tape (4905, 3M) or silicone elastomer (Sylgard 184 PDMS, Dow Corning) were brought into conformal contact with the silicon wafer. Pressure was manually applied, and the substrate was lifted to complete the transfer-printing. In other experiments (Fig. 5), the bGaIn was scraped off the silicon wafer and thoroughly hand-mixed. It was then patterned onto VHB tape (Fig. 5a) and paper (Fig. 5b) using a thin film applicator (Elcometer 3540), and directly written onto a piece of foam (Fig. 5c) and a latex balloon (Fig. 5d). Surface mounted LEDs (0603 package size, Kingbright) were adhered to the foam using cyanoacrylate (Loctite Instant-Bonding Adhesive 414, McMaster-Carr).

Electrical and mechanical characterization. The bGaIn resistance was measured using a four-point probe with a digital multimeter (5492B, BK Precision), after being transferred to a VHB substrate in a dog-bone pattern. The resistance values ($0.16 \pm 0.02\,\Omega$) were averaged from twelve measurements. The dog-bone patterns had an aspect ratio (length/width) of 5:1 (7.5×1.5 mm). Thicknesses of these patterns were measured using a three-dimensional optical profiler (Zygo Nexview), and averaged from twelve measurements (15.51 ± 1.55 µm). Initial conductivity of the biphasic material was calculated as $\sigma = l/Rwt = (2.06 \pm 0.29) \times 10^6$ S m^{-1}, where l, w, t and R are the length, width, thickness and resistance of the bGaIn patterns, respectively.

Contact resistance between bGaIn and electrical pins was measured using the transmission line method. An array of tinned copper contacts with various spacings was attached to a single bGaIn trace. Resistance values between each pair of contacts were measured. The measured contact resistance is half of the y intercept value of the linearly fitted line.

For electromechanical characterization, rectangular samples (length, 20 mm; width, 0.8 mm) were fabricated by transfer-printing bGaIn onto VHB or PDMS substrates. To eliminate the resistance changes at the interfaces between bGaIn and external wires, electrical connections were made by adhering copper tape on each end of the bGaIn traces, secured using silver conductive epoxy (Part no. 8331-14G, MG Chemicals). For the samples on PDMS substrates, fabric strips were placed at the interfaces to prevent stretching. The films were then encapsulated with another layer of VHB or PDMS. To test the circuits with bGaIn–component interfaces, zero-ohm resistors (1/10 W, 0603 package size, Yageo) were placed between two bGaIn traces. For VHB substrates, the resistors were held for 3 min to encourage bonding. For PDMS substrates, the resistors were placed when the silicone was only partially cured, and still 'tacky,' to enhance bonding. The two ends of the samples were clamped on three-dimensional printed parts and assembled on a customized tensile stage. The resistance values were measured using a Wheatstone bridge and corrected based on the clamped portion of the samples. The bGaIn samples were then subjected to uniaixal tensile loading at 15 mm min^{-1}, 150 mm min^{-1}, 225 mm min^{-1} or 300 mm min^{-1}.

Material characterization. Scanning electron microscopy images were taken by a Hitachi SU8230 ultra-high-resolution cold-field-emission scanning electron microscope. Samples for cross-section imaging were made by cleaving in liquid nitrogen. Elemental composition and mappings were obtained using energy dispersive X-ray spectroscopy (Flat-Quad, Bruker) at 5 kV. Optical imaging was performed using Zeiss Smartzoom 5. X-ray diffraction patterns were collected using a Rigaku Smartlab X-Ray diffractometer with CuKα radiation (8.04 keV, 1.5406 Å).

SCBA demonstration. The SCBAs shown in this work were fabricated by transfer-printing bGaIn onto VHB or silicone substrates with patterned masks. The masks were created by laser cutting liners of white matte sticker papers (Online Labels) using an ultraviolet laser micromachining system (Protolaser U4, LPKF) with 355 nm wavelength and 15 µm beam diameter. The glossy side of each liner was placed onto the VHB adhesive or silicone substrate, and easily peeled off after patterning. To provide electrical leads, tinned copper wires were flattened using a roller mill (Feiuruhf) and pressed onto the bGaIn contact pads. The VHB substrates were reinforced with double-sided tape, and the silicone substrates were reinforced with inextensible fabrics. Electrical wires were then soldered onto the flattened wires.

For the 'YALE' LED array, 33 LEDs (Kingbright, 0603) were pressed onto the VHB substrate at the designated positions and held for 3 min to encourage adhesion. The circuit was sealed with a layer of VHB on top. With voltage held constant at 2.7 V, the LED array was stretched to 250% strain by hand and then released.

The operational amplifier circuit consisted of a 14-pin rail-to-rail output operational amplifier (LMV 324, Texas Instruments). We supplied a 100 mV_{pp} sinusoidal signal with a 100 mV_{pp} offset and measured the output signals with an oscilloscope. The circuit was incrementally stretched, and the outputs were recorded at increments of 25% strain, up to 400%. As a control, the same circuit was built on a rigid copper-clad PCB board (G10/FR4, Pulsar) patterned by the LPKF laser, and tested with the same inputs at 0% strain.

The first-order resistor–capacitor low-pass filter circuit consisted of a resistor, a capacitor and bGaIn as electrical interconnects. We supplied a 500 mV_{pp} sinusoidal signal (V_{in}) at various frequencies and measured the output signals (V_{out}) with an oscilloscope. The circuit was incrementally stretched, and the outputs were recorded at increments of 100% strain, up to 400%. The magnitude in decibels (dB) was calculated as $20\log(\frac{V_{out}}{V_{in}})$. As a comparison, we created an identical circuit using eGaIn as electrical interconnects. The bGaIn was patterned as interfacial contacts for the eGaIn circuit to ensure stable connections with rigid electronic components.

The stretchable LED display was fabricated by first rod-coating a layer of silicone elastomer (Dragon Skin 10 Slow, Smooth-On) onto a polyethylene terephthalate (PET) substrate. Once the silicone cured, bGaIn was transfer-printed onto it to create the bottom circuit. Next, another layer of silicone elastomer was rod-coated on top and, after curing, another layer of bGaIn was printed. Once the top layer patterning was complete, 25 VIAs were created between the two layers by cutting cavities with an infrared laser (Universal Laser Systems VLS 2.30, 30 W, 10.6 µm CO_2 laser) and filling them with bGaIn. Then, 25 surface mounted LEDs (0603 package size, Kingbright) were bonded to the silicone elastomer layer using a silicone adhesive (Sil-Poxy, Smooth-On). Finally, the circuit was encapsulated by rod-coating another layer of silicone elastomer on top. The LEDs were controlled individually by an external microcontroller (Arduino Uno).

For the signal conditioning circuit board, an alignment fixture was built on an acrylic plate to achieve rapid and precise assembly of the top and bottom layers. VIA fabrication and transfer-printing methods were the same as in the other experiments. The circuit board included resistors, capacitors, a microcontroller (PIC16F1825, Microchip Technologies) and flattened tinned copper wires for interfacing with the stretch sensor and sending data to an external microcontroller (Arduino Uno). For characterization experiments, the signal conditioning circuit board was stretched and held at a certain strain using a customized tensile stage, while the capacitive sensor (1 cm wide with 105 mm gauge length) was subjected to ten cycles of repetitive strain from 0% to 50% using a materials tester (Instron 3345) at a strain rate of 150 mm min^{-1}. The sensor was secured to the materials tester via acrylic plates that had been sewn onto the ends of the sensor. The sensor was installed in a slack position, and the crosshead of the materials tester was raised until the sensors were not slack; no further pre-tension was applied to the sensors. For the sensory sleeve demonstration, the capacitive sensor was sewn onto a user's shirt sleeve and the signal conditioning circuit board was placed on the top of the sensor.

Data availability

Source data are provided with this paper. Other data supporting the findings of this study are available upon request from the corresponding author.

Acknowledgements

We acknowledge R. A. Bilodeau, M. C. Yuen and S. Y. Kim for their valuable comments on the manuscript; S. Wang for drawing the illustrations in Fig. 1e and Fig. 2a; L. Wang for access to the Zygo Nexview 3D Optical Profiler at the Yale West Campus Cleanroom; and M. Li for access to the scanning electron microscopy, energy dispersive spectroscopy and X-ray diffraction instruments at the Yale West Campus Materials Characterization Core and his advice on data analysis. S.L. was supported by the National Science Foundation (CAREER Award 1454284). D.S.S. was supported by a NASA (US National Aeronautics and Space Administration) Space Technology Research Fellowship (80NSSC17K0164).

Author contributions

S.L., D.S.S. and R.K.-B. conceived the project and planned the experiments. S.L. conducted all the experiments. D.S.S. programmed the PIC microcontroller for the signal conditioning circuit board demonstration. All authors participated in drafting and editing the manuscript. All authors contributed to, and agree with, the content of the final version of the manuscript.

Competing interests

The authors declare no competing interests.

Additional information

Supplementary information The online version contains supplementary material available at https://doi.org/10.1038/s41563-021-00921-8.

Correspondence and requests for materials should be addressed to R.K.-B.

Peer review information *Nature Materials* thanks Jaehong Lee, Tsuyoshi Sekitani and the other, anonymous, reviewer(s) for their contribution to the peer review of this work.

Reprints and permissions information is available at www.nature.com/reprints.